PHILOSOPHICAL TRANSACTIONS OF THE ROYAL SOCIETY A MATHEMATICAL, PHYSICAL & ENGINEERING SCIENCES

Rotational propensities in the state selection of NH^+_3 by pulsed–field ionization

H. Dickinson, D. Rolland and T. P. Softley

Phil. Trans. R. Soc. Lond. A 1997 **355**, 1585-1607
doi: 10.1098/rsta.1997.0078

Rotational propensities in the state selection of NH_3^+ by pulsed-field ionization

By H. Dickinson, D. Rolland and T. P. Softley

Physical and Theoretical Chemistry Laboratory, University of Oxford, South Parks Road, Oxford OX1 3QZ, UK

NH_3^+ ions have been prepared in unique vibration–rotation states v_2^+, N^+, K^+, by pulsed-field ionization of high Rydberg states of NH_3, populated by two-colour multiphoton excitation. The selected states, ranging from $v_2^+ = 0$ to 7 and N^+, $K^+ \leqslant 4$ are accessed via the B and C' states as intermediates. The application of multichannel quantum defect theory to the understanding of the rotational propensities in the mass-analysed threshold ionization spectra is discussed. It is demonstrated that the interactions of the Rydberg pseudo-continuum both with bound Rydberg states and with other continua can be modelled.

1. Introduction

In this paper we report on the selective preparation of NH_3^+ ions in well-defined vibration–rotation states $|v_2^+, N^+, K^+\rangle$ using pulsed-field ionization (PFI) of Rydberg states. We also discuss the application of multichannel quantum defect theory (MQDT) to the interpretation of rotational line intensities in the mass-analysed threshold ionization (MATI) and zero kinetic energy (ZEKE) photoelectron spectra. The long-term aim of this work is to study the reactions of quantum-state selected ions in bimolecular collision processes; this is a follow up to our previously reported results involving H_2^+, N_2^+, CO^+ and NO^+ (Merkt *et al.* 1993*b*; Mackenzie & Softley 1994; Mackenzie *et al.* 1995*a*,*b*, 1996; Softley *et al.* 1997*b*). The extending of the capabilities of the experiment to working with polyatomic ions provides, for example, the opportunity to investigate the effects of varying the projection quantum number K_a (and also K_c for asymmetric tops) on the reaction cross-section for processes such as $NH_3^+ + D_2 \rightarrow NH_3D^+ + H$. In effect, we are aiming to test whether the spinning top axial rotation has a greater or lesser effect compared to an end-over-end rotation about an axis perpendicular to the symmetry axis.

The technique we use has been described previously (Mackenzie & Softley 1994; Mackenzie *et al.* 1996) and is related to the ZEKE photoelectron and MATI spectroscopy techniques. In the present case the precursor neutral molecules are excited via a $2 + 1'$ two-colour resonance-enhanced multiphoton absorption using pulsed lasers. Rydberg states are produced in which the excited electron has an atomic-like principal quantum number of order $n = 150$–200, while the inner ion core has a well-defined set of quantum numbers v^+, N^+, K^+. Various different Rydberg series can be accessed with selected values of the core quantum numbers. After a time delay of a few μs to allow prompt ions to be separated by an applied electric field from the Rydberg state molecules (the prompt ions arise predominantly by one-colour

Phil. Trans. R. Soc. Lond. A (1997) **355**, 1585–1607
Printed in Great Britain

$2 + 1$ multiphoton ionization) the Rydberg states are field ionized by a small electric field to produce state-selected ions. As previously, we assert here that the field ionization leaves the ion core untouched leading to the production of a well-defined ionic quantum state, selected by tuning the lasers to the appropriate frequency. This assertion is discussed later in § 4. The state-selected ions are spatially separated from the prompt ions and their properties can then be investigated selectively. A significant feature of the work reported here is the ability, with relative ease, to produce the NH_3^+ ions in a wide range of vibrational states with 100% purity, using different intermediate vibrational levels of the B and C' intermediate states of NH_3.

Habenicht *et al.* (1991) previously reported the ZEKE photoelectron spectrum of NH_3 using $2+1'$ excitation via the B state level $v_2' = 2$ (where v_2' is the out-of-plane inversion mode). The same group also published (Reiser *et al.* 1993) a one-colour nonresonant two-photon ZEKE study involving excitation to $v_2^+ \geqslant 1$. Müller-Dethlefs subsequently presented a generalized theory for polyatomic rotational line intensities to try to account for the observed features in the spectrum and the apparent selection rules for angular momentum change (Müller-Dethlefs 1991). Although the model is partially successful, the ZEKE spectra show a number of features which are forbidden by the selection rules proposed in that work. In trying to extend the application of this model to explain more fully observations in PFI spectra via both the B and the C' states, we have adopted the formalism of multichannel quantum defect theory, following Child & Jungen (1990) and our previous MQDT calculations for the ZEKE spectra of H_2 (Softley & Hudson 1994). With the exception of some recent work on H_3 Rydberg states (Stephens & Greene 1995), this is the first time that MQDT has been applied to the rotational channel interactions in a symmetric top molecule (although the asymmetric top formalism of Child & Jungen (1990) uses a symmetric top basis set). Moreover, this work is an effort to extend the application of MQDT to the interpretation of ZEKE spectra beyond the realm of diatomic molecules.

An important feature of the spectra we have observed, in keeping with all our previous studies on diatomic molecules (Merkt & Softley 1993), is the presence of Rydberg channel interactions perturbing the spectra. The understanding of such interactions is much less developed for polyatomic molecules than for diatomics; the selection rules for inter-channel couplings are not well established, primarily because they are not generally observed explicitly, and only in NO_2 (Bryant *et al.* 1994) and H_2O (Gilbert & Child 1991) has there been clear evidence for their existence. In ZEKE spectra of most polyatomics the presence of such couplings appears to be obscured. The MQDT formalism permits quantitative inclusion and characterization of these effects.

2. Experimental

The apparatus used here, which was designed for studying state-selected ion–molecule reactions, has been described in more detail elsewhere (Mackenzie & Softley 1994; Mackenzie *et al.* 1996). Ammonia molecules are excited in a doubly skimmed pulsed supersonic beam using a two-colour resonance-enhanced multiphoton process. The beam stagnation pressure is 2 bar and a 1:10 mixture of NH_3 to Ar is expanded. The laser system consists of a dye laser (Spectra Physics PDL 3) and a BBO optical parametric oscillator system (MOPO 730) pumped by a single Nd:YAG laser (Quanta Ray GCR 290). The dye laser, pumped at 355 nm, operates in these experiments in the range 540–555 nm (3 mJ pulse^{-1}) for excitation via the C' state

and 430-445 nm (3 mJ pulse^{-1}) for excitation via the B state. The MOPO system, which is continuously tuneable over the range 690–430 nm, operates at 605–670 nm in these experiments and is frequency doubled using KD*P in an INRAD autotracking system to produce light at 302–335 nm (5 mJ pulse^{-1}). The two beams, which are temporally overlapped, are combined on a dichroic mirror and are then focused into the vacuum chamber using a 15 cm lens to intersect the molecular beam perpendicularly. The beam waist at the focal point is approximately 0.4 mm. Prompt ions are deflected out of the beam by applying a small perpendicular field (typically $F_d = 0.1$–0.5 V cm^{-1}), or alternatively they are retarded using a field parallel to the beam axis. The surviving Rydberg molecules continue, unaffected by the field, into the extraction region (with the exception of the very highest states which are field ionized) and then, after a suitable time delay, they are field ionized by a pulsed field (*ca.* 5 V cm^{-1}). The metastability of Rydberg states is crucial because it is necessary to allow a period of approximately 3.4 μs between excitation and field ionization to give adequate separation between Rydberg molecules and prompt ions. The extraction pulse accelerates the ions in the neutral beam direction and the ions are detected by a multichannel plate detector, arriving in a narrow time gate after passing along a 15 cm time-of-flight tube. To record $2 + 1$ REMPI spectra as a function of laser 1 wavelength (direct, above-threshold ionization in the final step rather than Rydberg excitation/field ionization), the discrimination field is switched off and all ions and Rydbergs are allowed to enter the extraction region, from which they are sent to the detector by the extraction pulse.

In the region between ion extraction and detection, there is a reaction zone in which the ions are moving through the molecular beam and can undergo reactive collisions with any neutral molecules present in the beam. The reaction zone is followed by a mass-selective quadrupole, the purpose of which is to select out product ions in studies of state-selective bimolecular reactions.

3. Experimental results

This section presents MATI spectra of ammonia via the B and C' resonant intermediate states. As stated in the introduction, the aim is to prepare NH_3^+ in unique vibration–rotation states v_2^+, N^+, K^+, where v_2^+, N^+ and K^+ represent the ion vibration (number of quanta in the v_2 inversion mode), rotation and molecule-fixed projection quantum numbers, respectively. A two-colour $(2 + 1')$ multiphoton excitation to high n Rydberg states is employed, followed by pulsed-field ionization. In order to achieve this aim there are three important factors.

(1) The MATI spectra must show well-resolved rotational lines.

(2) The transitions must have sufficient intensity to allow production of a usable population of state-selected ions.

(3) The pulsed-field ionization must proceed without perturbation of the ion core quantum state.

(*a*) *The one-colour REMPI spectrum of ammonia*

The $(2 + 1)$ resonance-enhanced multiphoton ionization spectrum of ammonia in the region $2\nu_1 = 60500$–66000 cm^{-1} is shown in figure 1. The spectrum shows a long progression in the v_2 'umbrella' bending mode due to the considerable change in geometry from the pyramidal ground state to the planar B and C' states. Previous photoelectron studies showed that the ionizing transitions are predominantly diag-

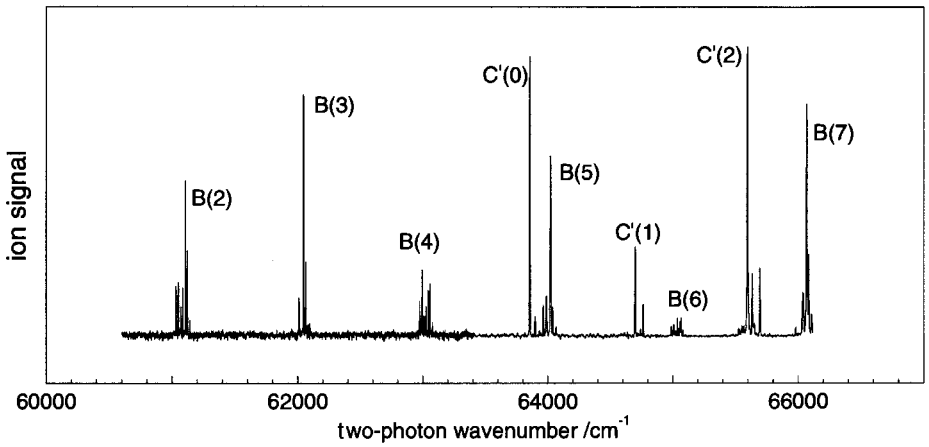

Figure 1. $2+1$ Resonance-enhanced multiphoton ionization spectrum of ammonia.

onal, with $> 70\%$ $\Delta v_2 = 0$ via the B state and $> 80\%$ $\Delta v_2 = 0$ via the C' state (Conway *et al.* 1985). This implies that by exciting to the high-n Rydbergs via the set of intermediate vibrational levels of both B and C' states shown in figure 1, ions in vibrational states with the same range of quantum numbers can be selected.

In the B and C' Rydberg states, and in the ion, the molecule is planar at equilibrium and D_{3h} is the appropriate symmetry group. The B and C' states have E'' and A_1' electronic symmetry overall, respectively, and because of the planar equilibrium geometry, they do not display the inversion doubling of the ground state. The v_2 vibration has A_1'' symmetry. Figure 2 shows the rotational energy levels for the B and C' states with their rovibronic symmetry labels, for odd and even numbers of quanta in the v_2 inversion mode. The requirement for the total wavefunction to be antisymmetric with respect to exchange of the ^{1}H nuclei implies that for a D_{3h} molecule, the overall symmetry must be A_2' or A_2''. The nuclear spin wavefunction $\psi_{\rm ns}$ can either have symmetry A_1 in ortho ammonia or E in para ammonia (ortho:para nuclear spin statistical weight ratio 2:1), so that, to give a total symmetry A_2, the rovibronic wavefunction $\psi_{\rm evr} = \psi_{\rm elec} \times \psi_{\rm vib} \times \psi_{\rm rot}$ must have either A_2 symmetry (ortho ammonia) or E symmetry (para ammonia). Consequently, states that would have A_1 rovibronic symmetry are not permitted.

Figure 3 shows the rotational structure in selected bands of the REMPI spectrum; the selection rules operating in the transitions to the intermediate state are the normal selection rules for two-photon optical transitions

$$\left.\begin{array}{c} \Delta J = 0, \pm 1, \pm 2, \\ C' \leftarrow X \text{ band (parallel)}, \quad \Delta K = 0, \\ B \leftarrow X \text{ band (perpendicular)} \quad \Delta K = \pm 1. \end{array}\right\} \tag{3.1}$$

In addition, due to the A_1'' symmetry of the transition dipole moment for rovibronic transitions (Bunker 1979), transitions to B and C' states with odd numbers of quanta in the v_2 vibration must come from the upper inversion doublet of the ground state, while transitions to states of even v_2 come from the lower component of the ground state doublet.

The simple appearance of the spectra is due to the significant rotational cooling of the molecular beam by the supersonic expansion (less than 15 K), which means that

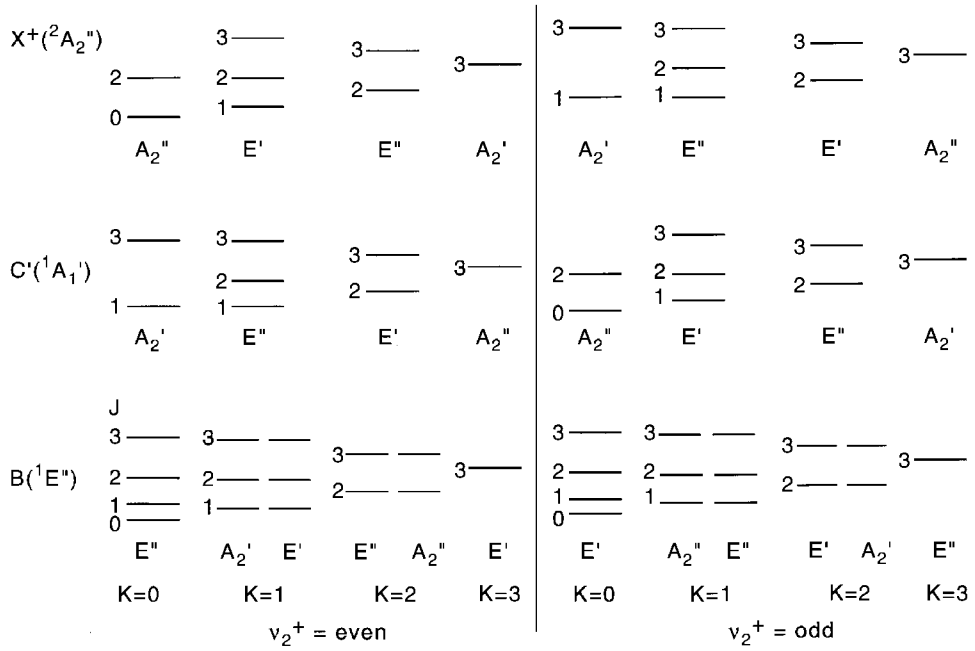

Figure 2. Rotational energy levels for the $B\,{}^1E''$ and $C'\,{}^1A_1'$ states (energies not to scale) and for the ionic ground state, $X\,{}^2A_2''$.

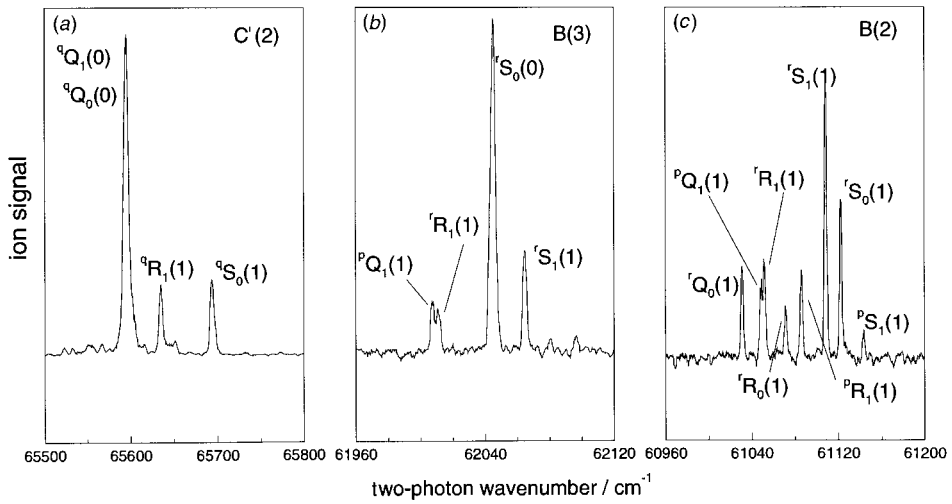

Figure 3. Rotational structure in the $2+1$ REMPI spectrum for various intermediate vibronic states: (*a*) $C'(v_2=2)$; (*b*) $B(v_2=3)$; (*c*) $B(v_2=2)$.

only the $(0,0)$, $(1,1)$ and $(1,0)$ levels of the ground state are significantly occupied (the notation used is (J,K)). Transitions were assigned by comparison with the work of Conaway *et al.* (1985) and by carrying out a simulation using the C' state constants from Nieman & Colson (1979) and Ashfold *et al.* (1984), and the B state constants and Hamiltonian from Ashfold *et al.* (1988).

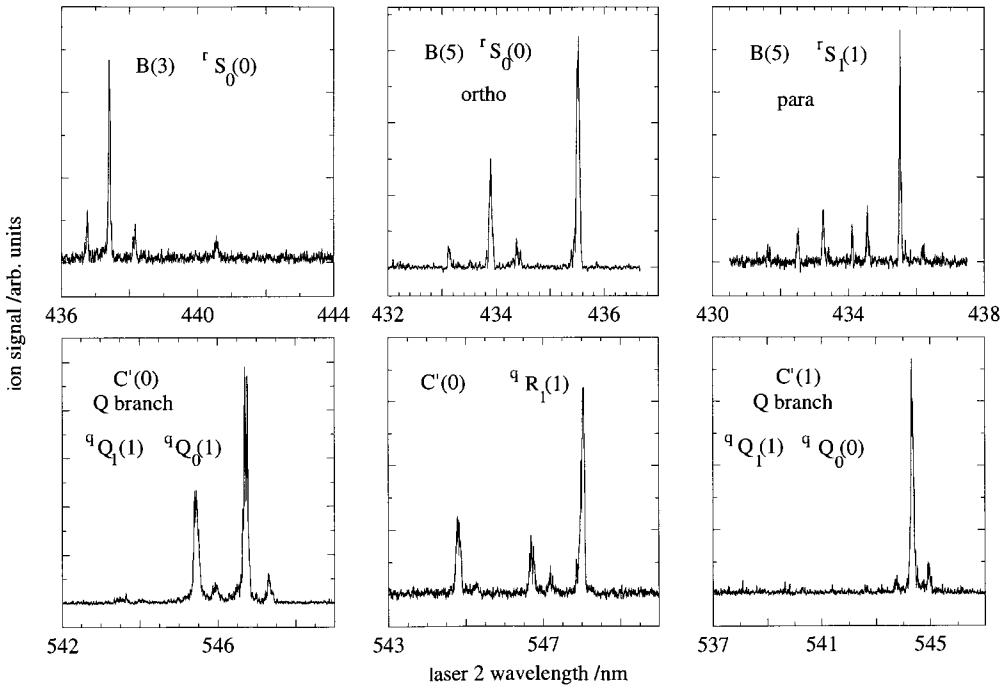

Figure 4. MATI spectra obtained from a range of intermediate vibronic levels of the B and C' states. The transitions are labelled with the transition to which laser 1 is tuned.

(*b*) *Recording of the MATI spectra of ammonia*

This section concentrates primarily on the MATI spectra obtained via the C' state of NH_3, although a sample of the spectra obtained via various intermediate levels of both B and C' states is shown in figure 4. Spectra obtained via the B state ($v_2 = 2$) have been reported previously (in a ZEKE experiment) by Habenicht *et al.* (1991) and further details of spectra we have obtained via the B state ($v_2 =$ 3–7) will be given in a future publication. The MATI spectra were recorded by applying a continuous discrimination field of 0.46 V cm^{-1} in the direction parallel to the molecular beam followed by a delayed pulsed field of 5 V cm^{-1}. It is found that the use of a significantly larger discrimination field leads to elimination of the MATI signal. The retarded fast ions arrive at the MCP later in time of flight than the pulsed field ionized (PFI) ions, so that the two may be distinguished. The balance of intensities between lasers 1 and 2 is critical. Excitation out of the intermediate state should be primarily by laser 2, yet laser 1 must provide sufficient intensity for a two-photon excitation to the intermediate to occur, but not so much that the transition is power broadened. In general we reduce the energy of laser 1 to around 1 mJ pulse^{-1}. To date, nearly all examples of multiphoton pulsed-field ionization photoelectron spectroscopy have been by $(1 + 1')$ schemes in which this balance is easier to attain.

In order to assign the observed spectra, the ionization thresholds corresponding to the various ionic rotation–vibration states were calculated from the simple formula

$$F(v_2^+, N^+, K^+) = G(v_2^+) + BN^+(N^+ + 1) + (C - B)K^{+2}. \qquad (3.2)$$

The rotational constants of the ion were taken from the work of Lee & Oka (1991). The MATI spectra recorded with laser 1 tuned to the $C(v_2 = 0) \leftarrow X$ Q branch

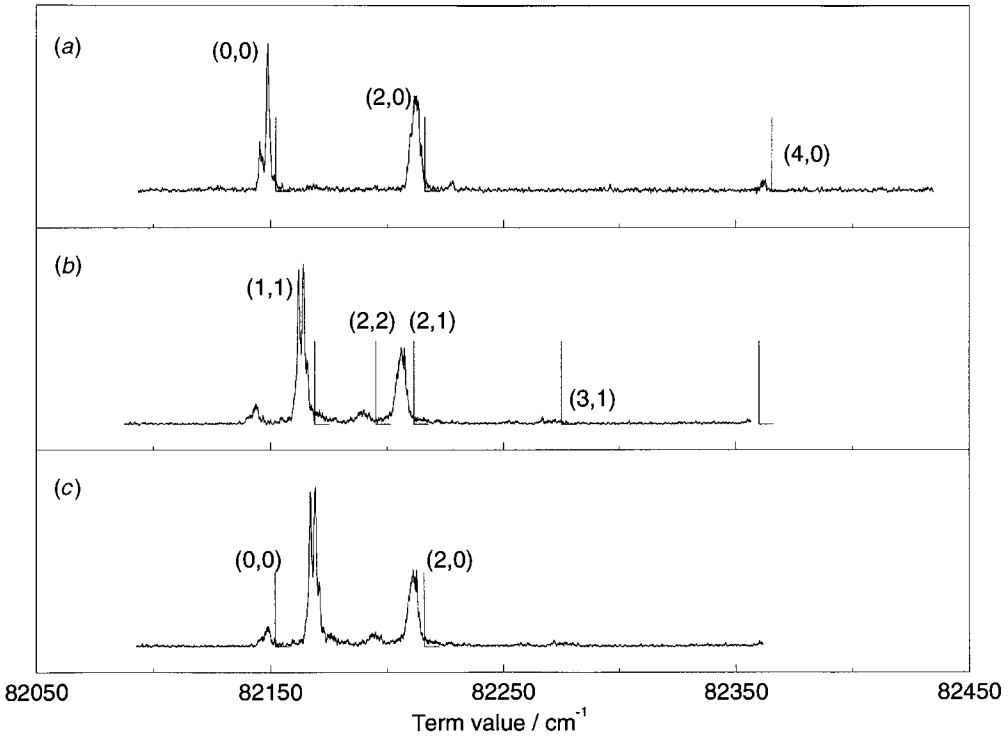

Figure 5. MATI spectra recorded via the $C'(v_2' = 0) \leftarrow X$ Q branch, with the laser 1 tuned to two-photon resonance at (*a*) 63 858.5 cm^{-1}; (*b*) and (*c*) 63 856.5 cm^{-1}. In (*b*) the term value (relative to $J = 0$, $K = 0$ in the ground state) is shown assuming the $(1, 1)$ intermediate level is populated, while in (*c*) the $(1, 0)$ intermediate is assumed.

are shown in figure 5. These spectra must be deconvoluted for the effect of two overlapping transitions in the Q branch; the ${}^qQ_0(1)$ and ${}^qQ_1(1)$ transitions populating the $C'(1, 0)$ and $C'(1, 1)$ states (labelled (J, K)). MATI spectra were recorded with laser 1 tuned to two different positions within the Q branch, at 63 858.5 cm^{-1} or 63 856.5 cm^{-1} (see figure 5). In the former case (figure 5*a*), the spectrum shows the peaks predicted by the selection rules (see § 5 *c*) for excitation out of the $C'(1, 0)$ state. This is to be expected, since the spectral constants for the ground and C' states predict the ${}^qQ_0(1)$ transition to $C'(1, 0)$ to be 1.6 cm^{-1} above the ${}^qQ_1(1)$ transition. The spectrum with laser 1 at 63 856.5 cm^{-1} appears to come mostly from the $C'(1, 1)$ state (figure 5*b*) but with weaker transitions from the $C'(1, 0)$ state showing through (figure 5*c*). The zero kinetic energy ionization thresholds for the peak assignments are indicated above each spectrum (labelled N^+, K^+) and, as expected, the PFI peaks are shifted to the red from these field free limits. The transitions observed all correspond to $K^+ - K' = 0$ with the exception of the weak $(2, 2)$ peak via $C'(1, 1)$.

The $(0, 0)$ and $(1, 1)$ peaks show fine structure with 2–3 sub peaks each. This is a characteristic signature of interactions between Rydberg series converging to different states of the ion. The interaction of the Rydberg electron with the core electrons at short range (or at longer range with the core quadrupole moment) can induce a pseudo-autoionization process in which a Rydberg state converging to one ionization threshold, say the $(2, 0)$, decays to an isoenergetic higher n Rydberg state converging on a lower threshold, say the $(0, 0)$, which is then field ionized (see figure 6). The

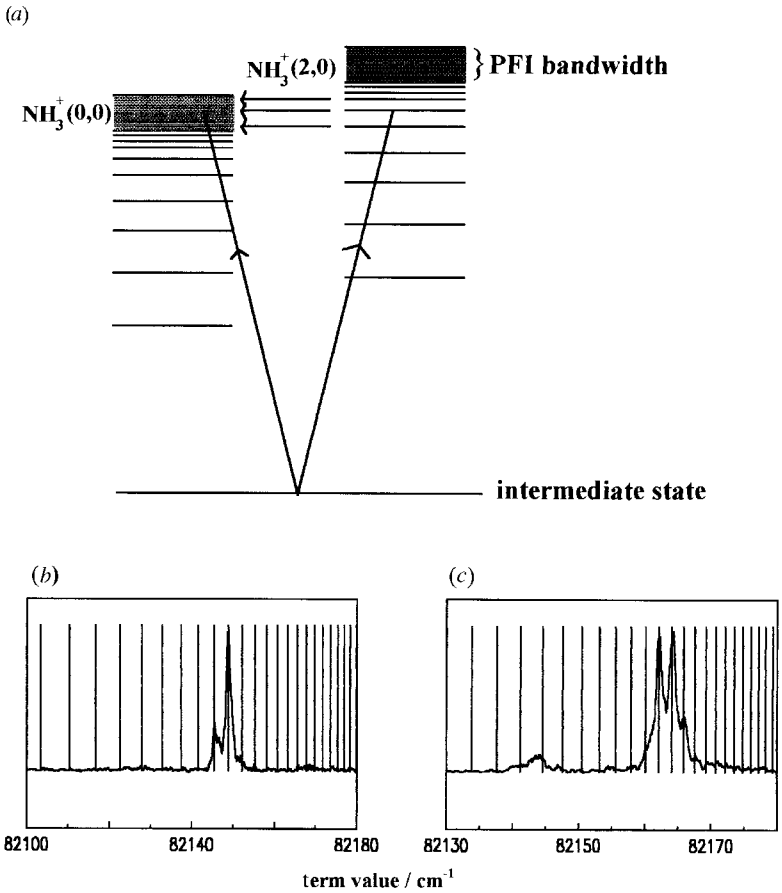

Figure 6. (*a*) Channel interactions in NH_3. (*b*) Sub-peaks in the $(0,0)$ peak from $C'(v_2=0)(1,0)$ intermediate fitted to the $(2,0)$ Rydberg series. (*c*) Sub-peaks in the $(1,1)$ peak from $C'(v_2=0)(1,1)$ fitted to the $(2,1)$ Rydberg series.

channel interaction causes intensity enhancements in the peak corresponding to the lower threshold, at the energies of Rydberg states converging to the higher threshold. The situation is directly analogous to a true autoionization as described by Fano (1964) for interactions between bound states (such as the interloper Rydbergs here) and true continua. For interaction of a single bound state with one continuum, the lineshape in the absorption spectrum was given by Fano in terms of the reduced energy variable ϵ as

$$\sigma(\epsilon) \propto \frac{(q+\epsilon)^2}{1+\epsilon^2}, \tag{3.3}$$

where the q parameter depends on the ratio of transition moments from the initial state ψ_0 to the zero-order bound state ϕ and to the zero-order continuum state ψ_{E}, and on the coupling strength $V_{\mathrm{E}} = \langle\psi_{\mathrm{E}}|H|\phi\rangle$:

$$q = \frac{\langle\psi_0|r|\phi\rangle}{\psi V_{\mathrm{E}}\langle\psi_0|r|\psi_{\mathrm{E}}\rangle}. \tag{3.4}$$

For the case of strong coupling and strong transition probability to the bound state,

$q \gg 1$ and a Lorentzian autoionization profile is obtained (an intensity enhancement in the continuum). For the case of weak transition probability to the bound state, $q \sim 0$ and a 'window resonance' is observed, corresponding to an intensity depletion.

As discussed below, the $(0,0)$ peak in figure 5 contains a *ca.* 50% contribution from the $\Delta N^+ = 2$ pseudo-autoionization process. The fine structure in the $(0,0)$ peak can be fitted to a Rydberg series converging to an ionic threshold at 82 217.5 cm^{-1}, using the formula

$$E_{\mathrm{nl}} = I(N^+, K^+) - \frac{R_y}{(n - \delta_{\mathrm{nl}})^2}, \tag{3.5}$$

with δ_{nl} from Glownia *et al.* (1980), assuming a d Rydberg series (see figure 6*b*). This ionization threshold is just above the energy of the $(2,0)$ peak in the spectrum and is clearly identified as the ionization threshold for the $(2,0)$ state of the ion, i.e. the channel interaction involves $\Delta N^+ = 2$, $\Delta K^+ = 0$. Using the spectral constants from Lee & Oka (1991) and this convergence limit, the ionization potential of ammonia in its ground rovibronic state is estimated to be 82 153.6 cm^{-1}. A channel interaction is also observed in the spectrum via the $C'(1,1)$ state, in which the $(1,1)$ peak shows fine structure superimposed on the MATI profile. This can be fitted to a Rydberg series converging to a threshold at 82 209.8 cm^{-1} (see figure 6*c*), presumably the $(2,1)$ threshold, i.e. in this case the channel interaction, involves $\Delta N^+ = 1$, $\Delta K^+ = 0$. This data can be used to calculate the ground state ionization potential as being at 82 151.3 cm^{-1}. Note that a $\Delta N^+ = 1$ interaction is not possible for the $(0,0)$ peak because (among other reasons) the $(1,0)$ channel does not exist, due to nuclear spin symmetry.

The MATI spectrum through the $C'(\nu_2 = 0)(2,1)$ state, pumped via the ${}^qR_1(1)$ line is shown in figure 7 and displays peaks corresponding to ions produced in the $(1,1)$, $(2,1)$ and $(3,1)$ rotational states. The $(3,1)$ peak is much stronger than in the spectrum via the $(1,1)$ intermediate state (figure 5*b*). Small additional peaks corresponding to the $(2,2)$ and $(3,2)$ states of the ion are also present. The fine structure in the $(1,1)$ peak is again observed as previously.

The MATI spectrum through the $C'(v_2 = 1)$ Q branch is shown in figure 8. In a similar way to the spectrum through the $C'(v_2 = 0)$ Q branch, this spectrum originates from two levels pumped simultaneously—the $C'(v_2 = 1)(0,0)$ state and the $C'(v_2 = 1)(1,1)$ state. The REMPI spectrum indicates that the ratio $(0,0)$ to $(1,1)$ is approximately 3:1, so the more intense features in the spectrum are expected to come from the $(0,0)$ intermediate. Figure 8 shows the spectrum plotted against term energy for excitation schemes via both intermediate states. The spectrum via $C'(v_2 = 1)(0,0)$ has as its principal feature a $(1,0)$ peak, with weak $(3,0)$ and $(3,3)$ peaks, while that via the $(1,1)$ level shows $(1,1)$ and $(2,1)$ peaks.

The MATI spectrum via the $C'(v_2 = 1)^qS_0(0)$ transition (the $(2,0)$ intermediate level) is shown in figure 9, with laser 1 tuned to 64764.2 cm^{-1}. It shows peaks due to formation of the $(1,0)$ and $(3,0)$ states of the ion. The $(3,0)$ peak is relatively much stronger from this $(2,0)$ intermediate than in the transition from the $(0,0)$ intermediate and the weak transition to the $(3,3)$ state is also more prominent. There again appears to be some intensity enhancement via a channel interaction in figure 9; there is an intense spike in the $(1,0)$ peak at a position calculated to correspond to the $n = 32$ Rydberg state of the $(3,0)$ series.

The shapes of the peaks in the spectra are definitive proof that channel interactions are occurring. This is the first time that channel interactions have been observed and well characterized in ZEKE or MATI spectrum of a molecule larger than a triatomic

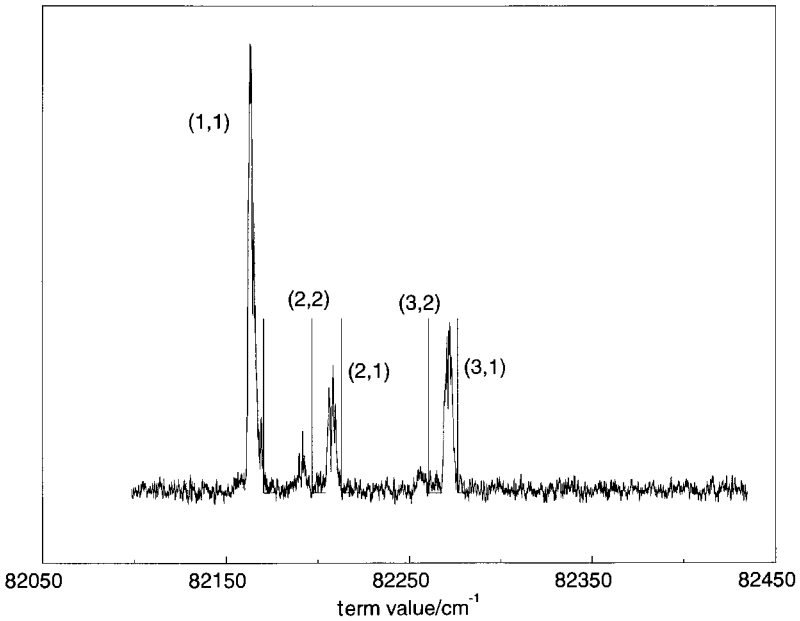

Figure 7. MATI spectra recorded via the $C'(v_2' = 0) \leftarrow X\ ^qR_1(1)$ line

and gives evidence that these may be a more universal phenomenon than is widely believed. These channel interactions, apart from their intrinsic interest, can be of assistance in producing more ions and a wider range of ionic quantum states.

(*c*) *Rotational state selection via the C′ state*

The MATI spectra described above via the C' state allow the ion states up to $N^+ = 4$ to be accessed. The following states can be formed completely state selectively (N^+, K^+):

$$\mathrm{NH_3^+}, v_2 = 0;\ (0,0), (1,1), (2,0), (2,1), (3,1), [(2,2), (4,0)\ \text{(only small numbers of ions formed)}],$$

$$\mathrm{NH_3^+}, v_2 = 1;\ (1,0), (1,1), (2,1), (3,0), [(3,3)\ \text{(only small numbers of ions formed)}].$$

In some cases, due to the superposition of two spectra when the Q branch is used as an intermediate, two states are formed simultaneously, e.g. the $C'(v_2 = 0)(2,0)$ and $(2,1)$ states.

4. Conservation of ionic core quantum numbers in field ionization

It is important to set down the arguments for why it is asserted that the field ionization process does not lead to any change of the ion core quantum state. The question here is whether the pseudo-continuum of Rydberg states belonging to the v^+, N^+, K^+ series is coupled by the delayed pulsed field to the v^+, N^+, K^+ continuum only, or whether the field in some way enhances the coupling to other continua, e.g. $v^+ - 1$, N^+, K^+ or v^+, $N^+ - 1$, K^+, etc., such that there is a non-zero branching ratio into other channels and hence a spoiling of the state selection. Of course, there may already be a coupling between the populated Rydberg states and these other

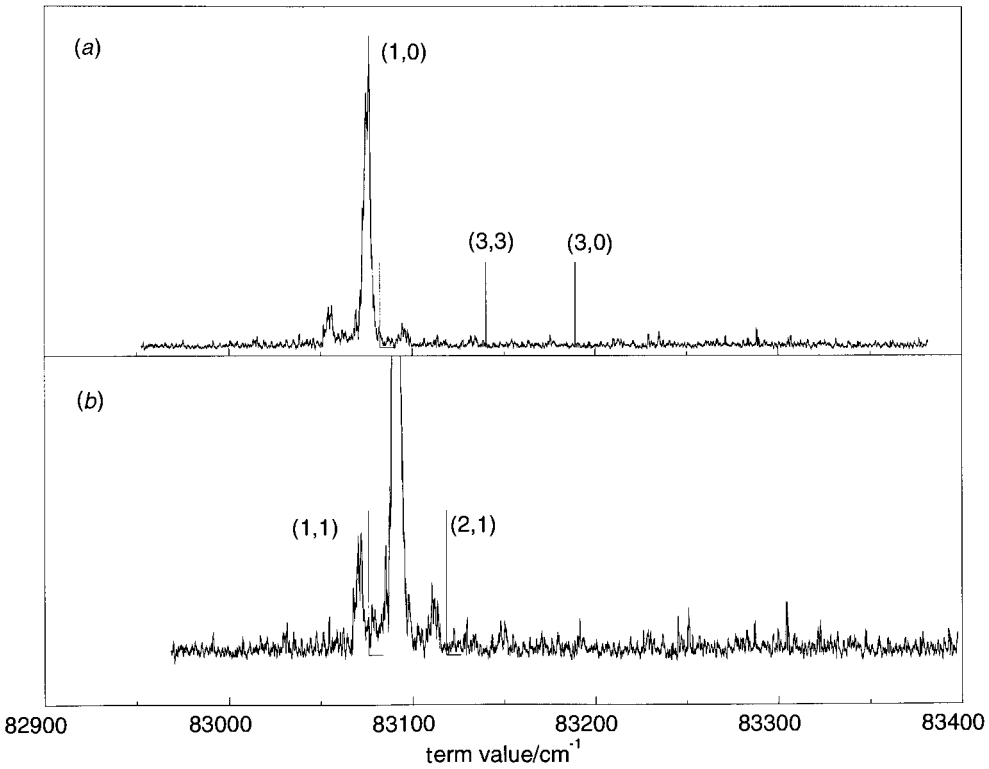

Figure 8. MATI spectra recorded via the $C'(v_2' = 1) \leftarrow X$ Q branch; term values assuming population of: (a) the $(0, 0)$ intermediate level; (b) the $(1, 1)$ intermediate.

continua before the pulsed field is applied. Such a coupling could lead to prompt ions, through autoionization, and if very slow, would add a long tail to the prompt ion time-of-flight signal. The fact that a significant proportion of Rydberg states *do* survive the initial decay time shows that, at least for a substantial fraction, the coupling to the continuum is very weak. However, the question here is whether the pulsed field applied could suddenly enhance the very weak couplings to these continua which had otherwise been very slow.

The long lifetime of the high-n Rydberg states has been acknowledged in recent years as one of the more surprising aspects of the ZEKE technique and has prompted considerable debate. It is now widely recognized that m_l mixing of the Rydberg states, caused by the presence of inhomogeneous fields experimentally, is a significant factor in diluting the coupling to the continuum (Merkt & Zare 1994; Chupka 1993). The long-lived Rydberg states must have a substantial degree of high m_l character and hence high-l character too. The Rydberg electron in such a state does not penetrate the core region and cannot undergo any exchange with the core leading to autoionization or predissociation. It then follows that if the pulsed field is to induce an additional coupling to other continua, it must lead to an admixture of low-m_l low-l character to allow core penetration. However, a homogeneous electric field cannot change the m_l quantum number and therefore cannot induce an admixture of low-l states (strictly speaking it is M_J the sum of $M_{N^+} + m_l$ which is conserved, however, m_l itself is approximately conserved.) Consequently it must be concluded that the

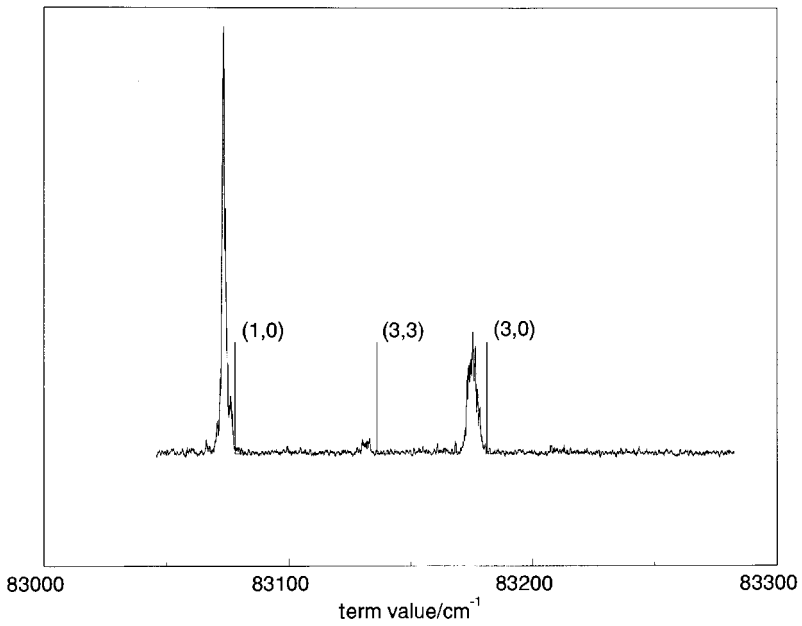

Figure 9. MATI spectra recorded via the $C'(v_2' = 1) \leftarrow X\ ^qS_0(0)$ line.

pulsed field does not induce any significant degree of coupling to other continua, especially as the competing direct field ionization must be very fast and therefore the ion core states remain well defined.

A second point is that if the pulsed field did induce additional couplings, then there would be no reason to suppose that these would simply be restricted to those states within the field ionization range, i.e. not only would the field ionized pseudo-continuum be coupled, but also lower lying Rydberg states could also be coupled. This would presumably lead to peaks in the ZEKE spectra that did not occur only within the well-defined limits of field ionization, i.e. the ZEKE peaks could be very much broader than predicted even by the $6.1\sqrt{F}$ law. In practice, there is no evidence for this behaviour. The ZEKE spectra observed for over 100 molecules rely on the well-defined field ionization behaviour to determine the resolution and we conclude that there is strong circumstantial evidence that field ionization proceeds directly to the continuum of the Rydberg series populated.

5. Rotational selection rules and intensities in the MATI spectrum of ammonia

ZEKE and MATI photoelectron spectroscopy have allowed rotational resolution in photoelectron spectra of a wide variety of molecules. Various approaches have been used to attempt to understand the rotational propensity rules and intensities observed. In the following section, we adopt an MQDT standpoint, combined with a modified version of the symmetry arguments used in the model of Müller-Dethlefs (1991); our model omits some of the symmetry correlations proposed in that paper. We believe that this model is the most promising way forward to understand the ZEKE and MATI spectra of ammonia via the B state and the C' state. Understanding the propensity rules is an important aid to assigning the spectra and our results

provide a test for the model. Moreover, given that there is mounting evidence that channel interactions have very widespread influence on ZEKE intensities, the development of methods to incorporate such effects is a crucial aspect of the evolution and applicability of this technique.

The key idea of the MQDT method is to divide the space of the Rydberg electron into two (or more) regions. In the long range region the Rydberg electron wavefunction is essentially hydrogenic—the potential is purely Coulombic—and the very weak coupling between the Rydberg electron and the ionic core angular momenta is well described by Hund's case (d). In this coupling case the valid quantum numbers for a symmetric top molecule, ignoring the electron spin, are: l, the Rydberg electron angular momentum quantum number; N, the total angular momentum of the molecule excluding spin; N^+, the angular momentum of the molecular core, i.e. the rotational quantum number of the ion formed; K^+, the component of the molecular core angular momentum on the symmetry axis; and M, the component of N on the space-fixed axis. For each N^+ there are $2l+1$ components of differing N ($N = N^+ + l, N^+ + l - 1, \ldots, N^+ - l$). In addition, it may be necessary to specify the vibrational and electronic quantum numbers of the ion core. It is also convenient to chose symmetrized linear combinations of these basis functions. Following Child & Jungen (1990), these are defined as

$$|N^+K^+p\rangle = \frac{[|NMlN^+K^+\rangle + (-1)^{p+N^++l}|NMlN^+ - K^+\rangle]}{[2(1+\delta_{K^+0})]^{1/2}}, \tag{5.1}$$

with p taking the values 0 or 1. Although the electron in a high-n Rydberg state spends most of its time in the long range region, it has a finite probability of moving close to the ionic core. In this short range region the wavefunction is more easily described as a linear combination of Hund's case (b) (or case (a)) functions. Furthermore, for a low-n Rydberg state (e.g. $n = 3$ or 4), the electron is most likely to be found in the core region and is therefore most closely described as case (a) or (b).

The valid quantum numbers in the Hund's case (b) representation are: λ, the component of the Rydberg electron orbital angular momentum l along the symmetry axis; N, the total angular momentum of the molecule excluding spin (equivalent to J for singlet states) as in Hund's case (d); K, the component of the rotational angular momentum of the molecule along the symmetry axis; and M, the component of N on the space-fixed axis. The Hund's case (d) quantum number K^+ is also well defined when K and λ are well defined, because the transformation between case (b) and case (d) requires $K = K^+ + \lambda$. The overall vibrational quantum numbers of the molecule may also be defined and, once again, it may be convenient to define symmetrized states using the 'parity' quantum numbers p_e and p_r such that

$$|\lambda K, p_\mathrm{e}, p_\mathrm{r}\rangle = \frac{[|l\lambda\rangle + (-1)^{p_\mathrm{e}}|l-\lambda\rangle][|NMK\rangle + (-1)^{p_\mathrm{r}+N}|NM-K\rangle]}{2[(1+\delta_{\lambda 0})(1+\delta_{K0})]^{1/2}}, \tag{5.2}$$

where p_r and p_e take the values 0 or 1. In fact, the linear combinations given here, following Child & Jungen (1990), are not distinguished by their properties under the E^* operation in the D_{3h} point group but actually, as far as the rotational part is concerned, by their behaviour under the $(23)^*$ operation. Nevertheless making this choice allows a clear relationship to be established between the D_{3h} rovibronic symmetry labels and the values of λ, p_e and p_r.

Although the electron may only spend a small amount of its time in the short range region, this case (b) range has particular significance in that: (i) the transition

moment is localized in this region; and (ii) all the non-hydrogenic interactions causing mixing of the long range channels originate from the behaviour at short range.

(*a*) *Zero-order model for the intensities*

In order to gain a full understanding of the observed intensities it is useful to start with a zero-order model, which ignores all channel interactions and gives the dominant propensity rules. This is obtained by assuming the final state in the two-colour excitation process is pure case (d), while the intermediate state from which the final excitation step takes place is pure Hund's case (b). The line strength I of a transition from the intermediate state ($''$) to the excited electronic state ($'$) represented in Hund's case (d) is given by

$$I = \sum_{M'M''} |\langle n'l'N^+K^+N'M'p'|\mu_z|l''\lambda''J''K''M''p''_{\rm e}p''_{\rm r}\rangle|^2, \tag{5.3}$$

where μ_z is the component of the dipole moment of the molecule along the space-fixed z-axis. The transition moment is evaluated by expressing the case (d) state as a linear combination of case (b) wavefunctions and therefore becomes a sum of case (b) transition moments. This is entirely appropriate in that, as already pointed out, the transition intensity is localized in the case (b) region.

$$\begin{aligned}\langle n'l'N^+K^+N'M'p'|\mu_z|l''\lambda''J''K''M''p''_{\rm e}p''_{\rm r}\rangle \\ = \sum_{\lambda'}\langle n'l'N^+K^+N'M'p'|n'l'\lambda'N'K'M'p'_{\rm e}p'_{\rm r}\rangle \\ \times\langle n'l'\lambda'N'K'M'p'_{\rm e}p'_{\rm r}|\mu_z|l''\lambda''J''K''M''p''_{\rm e}p''_{\rm r}\rangle.\end{aligned} \tag{5.4}$$

The transformation coefficient is given by equation (17) of Child & Jungen (1990) and, as shown by these authors, the transformation leads to the following expression for the Hund's case (d)–Hund's case (b) transition moment:

$$\begin{aligned}&\langle n'l'N^+K^+N'M'p'|\mu_z|l''\lambda''J''K''M''p''_{\rm e}p''_{\rm r}\rangle \\ &= \frac{(-1)^{l''+\lambda''}\sqrt{2}A(2N^+ + 1)^{1/2}}{[(1+\delta_{\lambda''0})(1+\delta_{K''0})(1+\delta_{K^+0})]^{1/2}}[\tfrac{1}{2}(1+(-1)^{p''_{\rm e}+p''_{\rm r}+p'+1})] \\ &\times \begin{pmatrix} l' & 1 & l'' \\ 0 & 0 & 0 \end{pmatrix} \begin{Bmatrix} J'' & l'' & N^+ \\ l' & N' & 1 \end{Bmatrix} \\ &\times \left\{ \left[\begin{pmatrix} l'' & N^+ & J'' \\ \lambda'' & K^+ & -K'' \end{pmatrix} + (-1)^{N^+ + l' + p'} \begin{pmatrix} l'' & N^+ & J'' \\ \lambda'' & -K^+ & -K'' \end{pmatrix} \right] \right. \\ &\left. + (-1)^{p''_{\rm e}} \left[\begin{pmatrix} l'' & N^+ & J'' \\ -\lambda'' & K^+ & -K'' \end{pmatrix} + (-1)^{N^+ + l' + p'} \begin{pmatrix} l'' & N^+ & J'' \\ -\lambda'' & -K^+ & -K'' \end{pmatrix} \right] \right\},\end{aligned} \tag{5.5}$$

with

$$A = \tfrac{1}{2}d_0[\tfrac{1}{3}(2N'+1)(2J''+1)(2l'+1)(2l''+1)]^{1/2} \tag{5.6}$$

and where d_0 is a one-electron radial integral, assumed to be independent of λ'. Note that K and λ only take positive values in the above equation.

In deriving expression (5.5), the electronic wavefunctions for the excited state and the intermediate state have been expanded as a product of an ion core electronic

function $\langle A_2''|$ and a Rydberg electron wavefunction $\langle l\lambda|$ allowing the electronic part of the transition moment to be written as

$$\langle A_2''|\langle l'\lambda'|\mu(1,q)|l''\lambda''\rangle|A_2''\rangle = \begin{pmatrix} l'' & 1 & l' \\ 0 & 0 & 0 \end{pmatrix} \begin{pmatrix} l'' & 1 & l' \\ -\lambda'' & q & \lambda' \end{pmatrix} [(2l'+1)(2l''+1)]^{1/2} d_0, \tag{5.7}$$

where $\mu(1,q)$ is a molecule fixed component of the dipole moment operator. Expression (5.5) immediately leads to a number of selection rules at this zero-order level of approximation, which should allow the prediction of the dominant transitions. First,

$$N^+_{\max} = J'' + l'', \quad N^+_{\min} = |J'' - l''|. \tag{5.8}$$

This selection rule for the change in total angular momentum from the intermediate state to the final state arises from the 3–j symbols in square brackets in equation (5.5). It expresses the conservation of angular momentum within the rotation spectator model (Merkt & Softley 1993; Merkt *et al.* 1993*c*), i.e. it is assumed that the angular momentum of the photon $\boldsymbol{\gamma}$ is consumed only by the excited electron, $\boldsymbol{l}'' + \boldsymbol{\gamma} = \boldsymbol{l}'$ (cf. equation (5.7)).

Secondly, from the bottom line of the 3–j symbols,

$$K^+ + \lambda'' = \pm K'' \quad \text{or} \quad |K^+ - \lambda''| = K'', \tag{5.9}$$

i.e. the maximum change in the K quantum number between the intermediate state and the final state is equal to the magnitude of λ'' in the intermediate state. Furthermore, it follows from equation (5.9) that (see also Child & Jungen 1990)

$$\text{for } \lambda'' = \text{even}, \quad K^+ - K'' = \text{even} \tag{5.10}$$

and

$$\text{for } \lambda'' = \text{odd}, \quad K^+ - K'' = \text{odd}. \tag{5.11}$$

The quantum number λ'' for the B and C' Rydberg states can be identified using descent of symmetry tables as given in Herzberg (1966). For the C' state, the overall electronic symmetry is A_1', which can be decomposed into the product of ion core and Rydberg electron symmetries:

$$\Gamma_{A_1'} = \Gamma_{\text{ion}} \times \Gamma_{\text{Ryd}} = A_2'' \times a_2''. \tag{5.12}$$

The a_2'' representation correlates with $\lambda = 0$ for l odd (e.g. pσ) or $\lambda = 3$ for l even (Herzberg 1966). It is fair to assume that the C' state can be represented as 100% pσ with no gϕ contribution. For excitation from the C' state we therefore obtain

$$K^+ - K'' = 0. \tag{5.13}$$

On the other hand, the B state has E'' symmetry, implying a Rydberg electron of e' symmetry, which correlates with $\lambda'' = 1$ for l odd (pπ), or $\lambda'' = 2$ for l even (dδ). Previous work has identified the orbital as predominantly pπ, but there is strong evidence presented below for non-negligible dδ character. In this case, a sum over the $l''\lambda''$ should be incorporated with an appropriate weighting coefficient within the square modulus of equation (5.3). The difference of character between the B and C' states has significant implications for the MATI spectra via these states and results in those via the C' state being somewhat more simple. It also means that the B state can be populated by one-photon absorption from the ground state whereas the C' state cannot. The pπ–dδ mixing should be considered as a short range configuration interaction within the core region.

The D_{3h} symmetry need otherwise only be considered explicitly to explain the nuclear spin effects. All other aspects of the symmetry are neatly encapsulated in the K and λ quantum numbers and the symmetrization quantum numbers. The nuclear spin species must be preserved in the final excitation step and this means that the transitions from the ortho levels (A_2 rovibronic symmetry) of the intermediate can only go to Rydberg series converging on the ortho levels of the ion ($K^+ = 0, 3, 6$). Likewise for para ammonia (E'' rovibronic symmetry) only the para K^+ levels can be populated ($1, 2, 4, 5 \ldots$). We also note that the levels $N^+ = 0, 2, 4$ do not exist for $v_2^+ =$ odd, $K^+ = 0$, while $N^+ = 1, 3, 5$ do not exist for $v_2^+ =$ even, as these would have A_1 symmetry.

(*b*) *Application of the zero order model to the spectra via the B state*

To illustrate the above, we consider first the application to the spectra reported in Habenicht *et al.* (1991) with excitation via the B state $v_2'' = 2$. From the *para* level $J'' = 3$, $K'' = 2$, one expects weak transitions to $K^+ = 4$ (para) originating from the $\lambda'' = 2$, dδ component (minor contribution to the intermediate wavefunction), using equations (5.9)–(5.11) and N^+ values of 4 or 5 from equation (5.8) (N^+ must be $\geqslant K^+$). From the $\lambda'' = 1$, pπ component of the intermediate (major contribution) one expects strong transitions to $K^+ = 1$ (para) with $N^+ = 2, 3, 4$. The experimental spectrum for the $(3, 2)$ para level (bottom figure 6 of Habenicht *et al.* (1991)) shows, for $v_2^+ = 2$, strong transitions to $K^+ = 1$ final states $N^+ = 2, 3, 4$ and weak transitions to $K^+ = 4$ with $N^+ = 4, 5$ in precise agreement with the above. The observation of the weaker components is very strong evidence for the significant but minor contribution of the dδ component.

Similarly, for the *ortho* level $J'' = 3$, $K'' = 1$, one would predict strong transitions from pπ to $K^+ = 0$, $N^+ = 2$ and 4 and weaker transitions from dδ to $K^+ = 3$, $N^+ = 3, 4, 5$. These transitions are indeed observed as described but the $N^+ = 0$, $K^+ = 0$ level is also observed weakly contrary to the rotation spectator approximation.

(*c*) *Application to the C′ state*

In applying these rules to the spectra via the C' state, we should expect

$$K^+ - K'' = 0 \tag{5.14}$$

and

$$N^+ = J'' + 1, J'', J'' - 1. \tag{5.15}$$

Table 1 confirms that these selection rules predict the strong components in the spectrum very well. However, a number of weak lines are observed, such as the transition to $(4, 0)$ from $v_2 = 0$ $(1, 0)$ and $(2, 2)$ from $v_2 = 0$ $(1, 1)$ which disobey the rules. Furthermore, there is clear evidence of channel mixing as discussed earlier through the appearance of fine structure in some of the peaks. Equation (5.5) is generally insufficient to predict the intensity ratios, either in the spectra via the B state or via the C' state. For example, the ratio of the $(0, 0)$ to $(2, 0)$ lines in figure 5 is predicted to be 1:2 not 1:1 as observed, and the $(4, 0)$ line should have no intensity.

The conclusion at this point is that the zero-order model is successful at predicting the dominant transitions, but does not give a complete understanding of the spectra. In the following section we build upon this zero-order model to take channel couplings into account.

Table 1. *Observed lines in the MATI spectra via various rotational levels of the* C' *state, compared with the predictions of the zero-order model*
([s] = strong, [w] = weak.)

C' level (J', K')	observed final states (N^+, K^+)	zero-order model predictions
$v_2' = 0$ $(1,0)$	$(0,0)$[s], $(2,0)$[s], $(4,0)$[w]	$(0,0)$ $(2,0)$
$v_2' = 0$ $(1,1)$	$(1,1)$[s], $(2,1)$[s], $(3,1)$[w], $(2,2)$[w]	$(1,1)$ $(2,1)$
$v_2' = 0$ $(2,1)$	$(1,1)$[s], $(2,1)$[s], $(3,1)$[s], $(3,2)$[w], $(2,2)$[w]	$(1,1)$ $(2,1)$ $(3,1)$
$v_2' = 1$ $(0,0)$	$(1,0)$[s], $(3,0)$[vw], $(3,3)$[w]	$(1,0)$
$v_2' = 1$ $(1,1)$	$(1,1)$[s], $(2,1)$[s]	$(1,1)$ $(2,1)$
$v_2' = 1$ $(2,0)$	$(1,0)$[s], $(3,0)$[s], $(3,3)$[w]	$(1,0)$ $(3,0)$

6. MQDT simulation of the spectra

(*a*) *Method*

The zero-order model outlined above is equivalent to assuming that all the quantum defects are exactly zero. In an MQDT approach, the Hund's case (d) functions in the outer region are matched at the core boundary to a linear combination of Hund's case (b) functions in the core region. In the zero quantum defect limit, the matching is given exactly by the transformation coefficients in equation (5.4) (see equation (17) of reference Child & Jungen (1990)). However, if the quantum defects are non-zero, the phase shifting of the wavefunctions in the core region changes the matching at the boundary, with the effect of inducing the channel interactions in the long range basis. The approach adopted in this work to incorporate non-zero quantum defects follows closely that described by Softley & Hudson (1994) and makes use of the transformations given in the previous section.

In outline, the pseudo-continuum of Rydberg states, which in the experiments is detected by field ionization, is treated as a true continuum. The relevant threshold is artificially lowered by *ca.* $10\,\mathrm{cm}^{-1}$ and we calculate the partial photoionization cross-section into that channel over the range corresponding to the field ionization. Following the methods described by Du & Greene (1986) and by Greene & Jungen (1985), the partial cross-section arising from a specific intermediate rotational level J'' is given by

$$\sigma_i(E) = \frac{4\pi^2\alpha\omega}{3(2J''+1)} \sum_{N'} |D_i^{(N'-)}(E)|^2, \tag{6.1}$$

where ω is the photon energy (AU). $D_i^{(N'-)}$ is a reduced dipole matrix element into a particular final channel iN', with i representing the set of quantum numbers l', N^+, K^+, and N' is the total angular momentum excluding spin. The parity p could also be included in the list represented by i but, for simplicity of presentation, we do not deal with that explicitly here. The reduced dipole matrix elements can be expressed as a linear combination of dipole matrix elements

$$D_i^{(N'-)} = \sum_{\rho} T_{i\rho} \exp(\mathrm{i}\pi\tau_\rho) D_\rho^{(N')}, \tag{6.2}$$

where τ_ρ and $T_{i\rho}$ are defined in equations (6.6) and (6.9) and

$$D_\rho^{(N')} = \sum_\alpha D_\alpha^{(N')} A_{\alpha\rho}. \tag{6.3}$$

The label ρ defines one of the N_o independent solutions of the Schrödinger equation at the energy E (see below), with N_o equal to the number of open channels at that energy. The wavefunctions $\Psi_\rho(E)$ have been expanded as a linear combination of 'eigenchannel solutions' labelled α, which in the present calculations are closely related to the Hund's case (b) basis set.

$$\Psi_\rho = \sum_{\alpha=1}^{N} A_{\alpha\rho}(E)\,\Psi_\alpha(E), \tag{6.4}$$

$$\Psi_\alpha(E) = \sum_i U_{i\alpha}[f_i \cos(\pi\mu_\alpha) - g_i \sin(\pi\mu_\alpha)]|i\rangle, \tag{6.5}$$

f_i and g_i are regular and irregular Coulomb functions, respectively. N is the total number of channels being considered, including both the open channels and the very large number (in principle) of closed channels. Also in equation (6.2),

$$T_{i\rho}(E) = \sum_{\alpha=1}^{N} U_{i\alpha}^{(N')} \cos\pi[-\tau_\rho + \mu_\alpha^{(N')}] A_{\alpha\rho}. \tag{6.6}$$

The μ_α and $U_{i\alpha}^{(N')}$ are the eigenvalues and eigenvectors of an $N \times N$ quantum defect matrix in the Hund's case (d) fragmentation channel basis set $(v^+N^+K^+N')$, whose elements are $\mu^{(N')}_{v^+N^+K^+,v^{+\prime}N^{+\prime}K^{+\prime}}$, where

$$\mu^{(N')}_{v^+N^+K^+,v^{+\prime}N^{+\prime}K^{+\prime}} = \sum_\lambda \langle N^+K^+|\lambda\rangle^{(lN')} \left[\int \mathrm{d}Q \langle v^+|Q\rangle^{(N^+)} \mu_\lambda(Q) \langle Q|v^{+\prime}\rangle^{(N^{+\prime})}\right] \times \langle\lambda|N^{+\prime}K^{+\prime}\rangle^{lN'}. \tag{6.7}$$

In this equation, the Hund's case (d) matrix elements have been related to the matrix elements in the Hund's case (b) representation via the transformation matrix element $\langle N^+K^+|\lambda\rangle^{(lN')}$ given by

$$\langle N^+K^+|\lambda\rangle^{lN'} = (-1)^{N'+\lambda-N^+}[2/(1+\delta_{\lambda 0})^{1/2}]\langle l - \lambda N'K'|N^+K^+\rangle \tag{6.8}$$

(cf. equation (17) of Child & Jungen (1990) for the full transformation including parity) and $\langle v^+|Q\rangle^{(N^+)}$ is the vibrational wavefunction of the ion core in the state v^+N^+. $\mu_\lambda(Q)$ is the quantum defect function in the Hund's case (b) representation and could be obtained in principle by subtracting the known potential surface for one of the low Rydberg states $nl\lambda$ of NH_3 from the potential energy surface of the ground state of NH_3^+. In the present preliminary work μ is taken to be independent of Q and therefore the term in square brackets in equation (6.7) becomes a single parameter μ_λ.

The eigenphases τ_ρ and the coefficients $A_{\alpha\rho}$ are obtained in the solution of a generalized eigenvalue equation at each energy.

$$\boldsymbol{\Gamma A} = \tan\pi\tau\boldsymbol{\Lambda A}, \tag{6.9}$$

$$\Gamma_{i\alpha} = U_{i\alpha}^{(N')} \sin\pi(\nu_i + \mu_\alpha^{(N')}), \quad \Lambda_{i\alpha} = 0, \quad \text{for } i \text{ closed}, \tag{6.10}$$

$$\Gamma_{i\alpha} = U_{i\alpha}^{(N')} \sin\pi\mu_\alpha^{(N')}, \quad \Lambda_{i\alpha} = U_{i\alpha}^{(N)} \cos\pi\mu_\alpha^{(N')}, \quad \text{for } i \text{ open}. \tag{6.11}$$

ν_i is the effective principal quantum number for the channel and energy of interest. The number of valid solutions to equation (6.9) is equal to the number of open channels. The ρth solution vector must be normalized according to

$$\sum_{i \text{ open}} \left(\sum_{\alpha=1}^{N} U_{i\alpha}^{(N')} \cos \pi [-\tau_\rho + \mu_\alpha^{(N')}] A_{\alpha_\rho} \right)^2 = 1. \tag{6.12}$$

The transition moments $D_\alpha^{(N')}$ in equation (6.3) are related by a sequence of frame transformations to the fixed-nuclei transition moments $d_\lambda(Q)$ in a Hund's case (b) basis set, via the transformation

$$D_\alpha^{(N')} = \sum_i (U^T)_{\alpha i}^{(N')} \sum_\lambda \langle N^+ K^+ | \lambda \rangle^{lN'} \left[\int \mathrm{d}Q \langle v^+ | Q \rangle^{(N^+)} d_\lambda(Q) \langle Q | v'' \rangle^{(J'')} \right]$$
$$\times \langle \lambda | J'' K'' \rangle^{lN'} (2N'+1)^{1/2}. \tag{6.13}$$

Here, $\langle Q|v''\rangle^{(J'')}$ is the vibrational wavefunction for the intermediate vibration–rotation energy level and $\langle \lambda | J'' K'' \rangle^{lN'}$ is given by equation (6.8). The term in square brackets was again approximated as a single parameter d_λ in this work.

(*b*) *Results of MQDT calculations*

For the preliminary calculations presented here we have attempted to simulate the spectrum shown in figure 5*a*. We consider the excitation of the 3pσ electron of the C' state into the $l = 2$ final channels only, with the $v_2^+ = 0$ $(1, 0)$ rotational level as the initial state. A 3-channel model is used which describes the interaction between the long-range channels $N^+ = 0, 2$ and 4 with $K^+ = 0$. These channels correspond to the three peaks shown in figure 5*a*. In Hund's case (b) this translates into the 3 'eigenchannels' d$\sigma(K = 0)$, d$\pi(K = 1)$ and d$\delta(K = 2)$. In this case, the transition intensity is non-zero only into the dσ and dπ channels and the relative magnitudes of the two transition moments d_π and d_σ are given by the value of the matrix element

$$\begin{pmatrix} l' & 1 & l'' \\ \lambda' & \nu & -\lambda'' \end{pmatrix},$$

where, for $\lambda'' = 0$, $\nu = -\lambda'$. The quantum defects $\mu_\lambda(l = 2)$ required in equation (6.3) are rather poorly determined from previous spectroscopic work for this system. From the term values given by Glownia *et al.* (1980), we evaluate these as given in table 2; the 3d values were used for the σ and δ components in this calculation. For the dπ quantum defect, which is unknown, we initially guessed the value $\delta = -0.02$. However, the predicted intensity of the $(4, 0)$ line is highly sensitive to the values of the quantum defects used and the most successful simulation, shown in figure 10, employed the value $\delta_\pi = 0.04$.

The simulation clearly displays the intensity enhancement of the $(0, 0)$ line, caused by interaction with the Rydberg states converging to the $(2, 0)$ limit, and the relative intensities of the $(0, 0)$, $(2, 0)$ and $(4, 0)$ lines are in close agreement with experiment. The origin of the intensity in the $(4, 0)$ peak, which should be zero according to the model presented in §§ 5 *a* and 5 *c*, is identified as being borrowed through the mixing of the $(4, 0)$ pseudo-continuum with the continua of the $(2, 0)$ and $(0, 0)$ channels. This simple simulation highlights one of the most important features of the MQDT formalism, namely its ability to represent continuum–continuum interactions, bound

Table 2. *Experimental quantum defects for p Rydberg states of ammonia*

Rydberg orbital	quantum defect
3dσ	−0.0491
4dσ	−0.0219
3dπ	
4dπ	
3dδ	−0.0101
4dδ	−0.057

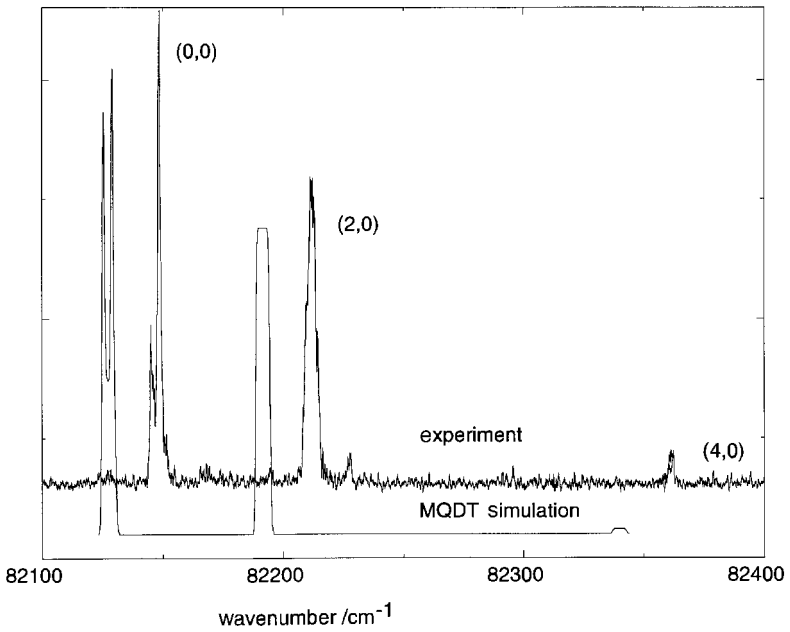

Figure 10. MQDT simulation of the MATI spectra from the $C'(v_2' = 0)(1, 0)$ level, compared with the experimental spectrum. The simulation has been shifted by 20 cm^{-1} for clarity of presentation.

state–bound state interactions and bound state–continuum interactions in a single calculation. The clear identification of intensity borrowing from the continuum is an unusual feature of these results, although it is one which is implicit in much of the work applied to other systems by McKoy and co-workers (Müller-Dethlefs *et al.* 1995).

These preliminary results are highly encouraging. In view of the substantial amount of data available from the NH_3 ZEKE and MATI spectra via a wide range of intermediate states, there are good prospects for our being able to characterize this system in detail and derive well-defined values for the quantum defect parameters; a full analysis will be presented in a future publication. It should be noted that the appearance of the weak $\Delta K = 1$ lines in the spectrum shown in figure 7 leads to the necessity to incorporate p–d channel mixing in the final state. Such an interaction has already been identified as important in the B intermediate state and

arises because the p($\lambda = 1$) and d($\lambda = 2$) components have the same symmetry (e'). The origin of this effect is best thought of as a short range configuration interaction within the core region, rather than as a long range mixing induced by the ion core quadrupole.

A final question to be asked is whether these zero-field MQDT calculations are reliable when dealing with high-n Rydberg states, because of the likely influence of stray electric fields, which might lead to additional couplings. In an earlier publication we have suggested that electric-field induced couplings are not likely to be important in molecules with large rotational constants (Merkt *et al.* 1993*a*). Very recently we have shown in a 200 channel MQDT calculation (Softley *et al.* 1997*a*), including the effects of electric fields, that channel interactions in hydrogen, such as the 26p2 $v^+ = 2$ window resonance interacting with the $v^+ = 2$ $N^+ = 0$ pseudo-continuum are maintained in the presence of an electric field which is substantially above the Inglis Teller limit for the pseudo-continuum. This situation is likely to be general, at least in systems with non-dipolar cores, provided that the interaction width with the pseudo-continuum exceeds the zero-field level spacings.

7. Conclusion

In this paper we have demonstrated the possibility for state selection of NH_3^+ ions in well-defined vibration–rotation quantum states. An important challenge for the success of these experiments is to produce sufficient ions to study the subsequent reactions and therefore the understanding of intensities is an essential aspect of the work. The spectra show strong evidence for channel interactions with bound Rydberg states, making the interpretation of intensities difficult using conventional methods applied to photoelectron spectra. This difficulty is not unique to this molecule but is found in many small molecules, and possibly larger ones too. We have demonstrated in a preliminary calculation that MQDT provides a way forward to the interpretation and prediction of the intensities and we believe that this method will be applicable ultimately well beyond the realm of small diatomic molecules.

References

Ashfold, M. N. R., Dixon, R. N. & Stickland, R. J. 1984 Molecular predissociation dynamics revealed through multiphoton ionization spectroscopy of the C' states of NH_3 and ND_3. *Chem. Phys.* **88**, 463–478.

Ashfold, M. N. R., Dixon, R. N., Little, N., Stickland, R. J. & Western, C. M. 1988 The B^1E'' state of ammonia: sub-Doppler spectroscopy at vacuum ultraviolet energies. *J. Chem. Phys.* **89**, 1754–1761.

Bryant, G. P., Jiang, Y., Martin, M. & Grant, E. R. 1994 Rovibrational structure of NO_2^+ and state-to-state dynamics in the high-resolution threshold photoionization of NO_2. *J. Chem. Phys.* **101**, 7199–7210.

Bunker, P. R. 1979 *Molecular symmetry and spectroscopy.* New York: Academic.

Child, M. S. & Jungen, Ch. 1990 Quantum defect theory for asymmetric tops: application to the Rydberg states of H_2O. *J. Chem. Phys.* **93**, 7756–7766.

Chupka, W. A. 1993 Factors affecting lifetimes and resolution of Rydberg states observed in zero-electron-kinetic-energy spectroscopy. *J. Chem. Phys.* **98**, 4520–4530.

Conaway, W. E., Morrison, R. J. S. & Zare, R. N. 1985 Vibrational state selection of ammonia ions using resonant $2 + 1$ multiphoton ionization. *Chem. Phys. Lett.* **113**, 429–434.

Du, N. Y. & Greene, C. H. 1986 Quantum defect analysis of HD photoionization. *J. Chem. Phys.* **85**, 5430–5436.

Fano, U. 1964 Effects of configuration interaction on intensities and phase shifts. *Phys. Rev.* **124**, 1866–1878.

Gilbert, R. & Child, M. S. 1991 Effects of polarization in the field ionization spectrum of H_2O. *Chem. Phys. Lett.* **287**, 153–160.

Glownia, J. H., Riley, S. J., Colson, S. D. & Nieman, G. C. 1980 The MPI spectrum of expansion cooled ammonia: photophysics and new assignments of electronic excited states. *J. Chem. Phys.* **73**, 4296–4309.

Greene, C. H. & Jungen, Ch. 1985 Molecular applications of quantum defect theory. *Adv. At. Mol. Phys.* **21**, 51–121.

Habenicht, W., Reiser, G. & Müller-Dethlefs, K. 1991 High resolution zero kinetic energy electron spectroscopy of ammonia. *J. Chem. Phys.* **95**, 4809–4819.

Herzberg, G. 1966 Molecular spectra and molecular structure. In *Electronic spectra and electronic structure of polyatomic molecules*, vol. 3. Princeton, NJ: Van Nostrand.

Lee, S. S. & Oka, T. 1991 Diode laser spectroscopy of the v_2 fundamental and hot bands of NH_3^+. *J. Chem. Phys.* **94**, 1698–1704.

Mackenzie, S. R. & Softley, T. P. 1994 New experimental method for studying rotationally state-selected ion–molecule reactions. *J. Chem. Phys.* **101** 10609–10617.

Mackenzie, S. R., Halse, E. J., Merkt, F. & Softley, T. P. 1995*a* Rotationally state-selected ion–molecule reactions studied using pulsed-field ionization techniques *Proc. SPIE* **2548**, 293–304.

Mackenzie, S. R., Halse, E. J., Merkt, F. & Softley, T. P. 1995*b* Rotational state-selectivity in $N_2^+ X\,^2\Sigma_g^+$ ($v^+ = 0$) by delayed pulsed-field ionization (PFI) spectroscopy via the $a''\,^1\Sigma_g^+$ ($v' = 0$) state. *Molec. Phys.* **86**, 1283–1297.

Mackenzie, S. R., Halse, E. J., Gordon, E., Rolland, D. & Softley, T. P. 1996 Pulsed-field ionization spectroscopy of CO via the $E\,^1\Pi$ state and NO via the $B\,^2\Pi$ state. *Chem. Phys.* **209**, 127–142.

Merkt, F. & Softley, T. P. 1993 Rotational line intensities in zero kinetic energy photoelectron spectroscopy (ZEKE-PES). *Int. Rev. Phys. Chem.* **12**, 205–239.

Merkt, F., Fielding, H. H. & Softley, T. P. 1993*a* Electric field effects on zero-kinetic energy photoelectron spectra: an explanation of observed trends. *Chem. Phys. Lett.* **202**, 153–160.

Merkt, F., Mackenzie, S. R. & Softley, T. P. 1993*b* Preparation of ions in selected rotational states by delayed pulsed field ionization. *J. Chem. Phys.* **99**, 4213–4214.

Merkt, F., Mackenzie, S. R., Rednall, R. J. & Softley, T. P. 1993*c* Zero-kinetic-energy photoelectron spectrum of carbon dioxide. *J. Chem. Phys.* **99**, 8430–8439.

Merkt, F. & Zare, R. N. 1994 On the lifetimes of Rydberg states probed by delayed pulsed-field ionization. *J. Chem. Phys.* **101**, 3495–3505.

Müller-Dethlefs, K. 1991 Zero kinetic energy electron spectroscopy of molecules: rotational symmetry selection rules and intensities. *J. Chem. Phys.* **95**, 4821–4839.

Müller-Dethlefs, K., Schlag, E. W., Grant, E., Wang, K. & McKoy, V. 1995 ZEKE spectroscopy: high resolution spectroscopy with photoelectrons. *Adv. Chem. Phys.* **90**, 1–104.

Nieman G. C. & Colson, S. D. 1979 Characterization of the C' state of ammonia observed by three-photon gas phase spectroscopy. *J. Chem. Phys.* **71**, 571–577.

Reiser, G., Habenicht, W. & Müller-Dethlefs, K. 1993 Zero kinetic energy (ZEKE) photoelectron spectroscopy of ammonia by nonresonant two-photon ionization from the neutral ground state. *J. Chem. Phys.* **98**, 8462–8467.

Softley, T. P. & Hudson, A. J. 1994 Multichannel quantum defect theory simulation of the ZEKE photoelectron spectrum of H_2. *J. Chem. Phys.* **101**, 923–928.

Softley, T. P., Hudson, A. J. & Watson, R. 1997*a* Multichannel quantum defect theory Stark effect calculation of autoionization lifetimes in high-n Rydberg states of Ar, N_2 and H_2. *J. Chem. Phys.* **106**, 1041–1056.

Softley, T. P., Mackenzie, S. R., Merkt, F. & Rolland, D. 1997*b* From Rydberg state dynamics to ion–molecule reactions using ZEKE spectroscopy. *Adv. Chem. Phys* **101**, 667–698.

Stephens, J. A. & Greene, C. H. 1995 Rydberg state dynamics of rotating vibrating H_3 and the Jahn–Teller effect. *J. Chem. Phys.* **102**, 1579–1591.

Discussion

M. J. J. Vrakking (*FOM Institute for Atomic and Molecular Physics (AMOLF), Amsterdam, The Netherlands*). In his experiments on Xe Dr Softley reported the observation of a low-n component in the Xe pulsed field ionization spectrum, which he attributed to charge transfer to surrounding Xe ions, similar to the mechanism reported in some of the experiments by Professor Schlag. Has he tried to characterize this process further by, for example, determining the lifetimes of these states? As he may recall, in our experiments on Xe in Berkeley (Vrakking & Lee 1995), we saw Rydberg states with extremely long lifetimes (many microseconds) following excitation of the autoionizing Rydberg series at relatively low-n, where the kinetic energy distribution of the Rydberg atom indicated that the spin-orbit energy of the initially excited Rydberg state had been made available in the collision between two Xe atoms. Is it possible that this mechanism plays a role in his experiments?

T. P. Softley. At the present time we have not tried to identify the spin-orbit state of the Rydberg core, nor to study the lifetimes of the states which are eventually ionized either by a small pulsed field or by SF_6 electron attachment. However, the time delay used for the pulsed field ionization was approximately 1 μs and the average collision time in the SF_6 experiments was of similar order, so that it is apparent that the Xe Rydberg atoms become highly stabilized. These observations could therefore be consistent with Dr Vrakking's previous studies.

M. J. J. Vrakking. Dr Softley presented studies of the collision energy dependence of state-selected ion–molecule reactions, which, in agreement with the Langevin model, show that the cross-section peaks at low collision energy, and then rapidly drops towards higher collision energies. In order to carry out the experiment at a high collision energy, one has to accelerate the state-selected ions, and thereby take them through the region of high collision cross-section. Is this a problem?

T. P. Softley. The collisions during acceleration turn out to be not so much of a problem as might first be expected. The probability that during the short acceleration period, typically *ca.* 100 ns, the ion comes within a few collision diameters of a neutral molecule is actually very small under the conditions of our experiment and always less than 2% (defining the collision diameters as given by the Langevin formalism for a relative velocity in mid-acceleration). Thus, although lower energy collisions cannot be ruled out completely, under most circumstances here we believe they can be neglected.

A. Dalgarno (*CFA, Harvard University, USA*). Does Dr Softley have any information on the rotational and vibrational structure of the product H_3^+ ion in the reaction $H_2^+ + H_2 \rightarrow H_3^+ + H$? Will he be able to measure the cross-sections of the reaction $NH_3^+ + H_2 \rightarrow NH_4^+ + H$?

T. P. Softley. At the present time, the quantities of product ions produced are so small that direct spectroscopic measurement of the vibration–rotation distribution would be impossible. However, it may be possible to obtain the information indirectly in the near future by measuring the kinetic energy distribution of the product ions. The reaction of NH_3^+ with H_2 is amongst those that we intend to study, although absolute cross-sections may be difficult to obtain in the present experimental set up.

Additional references

Vrakking, M. J. J. & Lee, Y. T. 1995 *J. Chem. Phys.* **102**, 8833.

PHILOSOPHICAL TRANSACTIONS OF THE ROYAL SOCIETY A MATHEMATICAL, PHYSICAL & ENGINEERING SCIENCES